A Vortical Boundary Layer for Near-Radial IMF: Wind Observations on October 24, 2001

C. J. Farrugia,[1] F. T. Gratton,[2, 3] G. Gnavi,[2] R. B. Torbert,[1,4] Lynn B. Wilson III[4]

C. J. Farrugia, R. B. Torbert, Space Science Center and Department of Physics, University of New Hampshire, Durham, NH (charlie.farrugia@unh.edu)

G. Gnavi, F. T. Gratton, Instituto de Física del Plasma, Consejo Nacional de Investigaciones Científicas y Técnicas, Universidad de Buenos Aires, 1428 Buenos Aires, Argentina; and Departamento de Física, Facultad de Ciencias Fisicomatemáticas e Ingeniería, Pontificia Universidad Católica Argentina, Buenos Aires, Argentina.

L. B. Wilson III, NASA-Goddard Space Flight Center, Greenbelt, MD

[1]Space Science Center and Department of

Abstract. We present an example of a boundary layer tailward of the dawn terminator which is entirely populated by rolled-up flow vortices. Observations were made by Wind on October 24, 2001 as the spacecraft moved across the region at X ∼-13 R_E. Interplanetary conditions were steady with a near-radial IMF. Approximately 15 vortices were observed over the 1.5 hr duration of Wind's crossing, each lasting ∼5 min. The rolling-up is inferred from the presence of a hot tenuous plasma being accelerated to speeds higher than in the adjoining magnetosheath, a circumstance which has been shown to be a reliable signature of this in single-spacecraft observations [*Takagi et*

Physics, University of New Hampshire,

Durham, NH, USA

[2]Instituto de Física del Plasma, Consejo Nacional de Investigaciones Científicas y Técnicas, Universidad de Buenos Aires, 1428 Buenos Aires,Argentina

[3]Departamento de Física, Facultad de Ciencias Fisicomatemáticas e Ingeniería, Pontificia Universidad Católica Argentina, Buenos Aires, Argentina

[4]NASA/Goddard Space Flight Center, Greenbelt, MD.

al., 2006]. A blob of cold dense plasma was entrained in each vortex, at whose leading edge abrupt polarity changes of field and velocity components at current sheets were regularly observed. In the frame of the average boundary layer velocity, the dense blobs were moving predominantly sunward and their scale size along X was $\sim 8.4\ R_E$. Inquiring into the generation mechanism of the vortices, we analyze the stability of the boundary layer to sheared flows using compressible magnetohydrodynamic Kelvin–Helmholtz theory with continuous profiles for the physical quantities. We input parameters from (i) the exact theory of magnetosheath flow under aligned solar wind field and flow vectors [Spreiter and Rizzi, 1974] near the terminator, and (ii) the Wind data. It is shown that the configuration is indeed KH unstable. This is the first reported example of KH-unstable waves at the magnetopause under a radial IMF.

1. Introduction

There is a long history of observations of waves at the boundary between the magnetosphere and the magnetosheath (e.g. [*Lepping and Burlaga*, 1979]; [*Sckopke et al.*, 1981], [*Chen and Kivelson*, 1993]; [*Farrugia et al.*, 2001], and references therein). In view of the velocity shear that exists between these two plasma regimes, the Kelvin-Helmholtz (KH) instability has often been invoked to explain these waves.

From theoretical studies of the KH instability, two main points to keep in mind are the following: (i) the magnetic tension force (analogous to the surface tension force in hydrodynamics); and (ii) the compressibility of the plasma. Both are stabilizing factors. Thus KH instability depends on the magnetic field configurations, in particular their orientations with respect to the flow, and the speed of the plasma, which increases with distance down the flanks.

KH waves are thought to be one way of transferring solar wind momentum and energy to the magnetosphere. The KH instability forms part of the so-called "*viscous-type*" solar wind–magnetosphere interactions, to distinguish them from reconnection between the magnetosheath and magnetosphere fields. The contribution of viscous-type interactions to the cross-polar cap potential is often estimated as $\sim$ 30 kV [*Cowley*, 1982]. The question of magnetosheath mass entry goes beyond considerations of ideal MHD stability since other processes are required to break the associated frozen-in condition. However, the large vortices generated by the KH instability may set up conditions favorable to small-scale tearing of magnetic field lines inside the structures and, as a consequence, to mass diffusion (see e.g. *Otto and Fairfield*, [2000]; *Smets et al.*, [2002]; *Otto and Nykyri*, [2003]).

Many of the data examples of KH instability in a magnetospheric context have used the capability of multiple spacecraft observations, such as Cluster, to confirm the presence of waves and their features, in particular if they have reached a non-linear phase and started to roll over. However, we do not often have this luxury and there are many tabulated crossings of a wavy magnetopause boundary made by single spacecraft. Can we somehow infer the presence of rolled–up vortices from single–spacecraft observations?

A key advance in this direction was made by *Takagi et al.* [2006]. Their MHD simulations showed that *in situ* observations of a low density magnetospheric plasma moving tailward at speeds higher than that of the adjacent magnetosheath is a very good indicator of rolled-up vortices. This opens new possibilities. First to apply this criterion were *Hasegawa et al.* [2006], who confirmed results on rolled-up KH vortices obtained earlier by *Hasegawa et al.* [2004] with a multi-spacecraft analysis. While the simulations were done for a northward IMF and specific parameters characterizing the ambient regions, *Nakamura et al.* [2004] had already given the physical origin of the signature of a rolled-up vortex. For pressure balance to hold across the vortex (same centrifugal forces at a given radial distance from the center), the hot tenuous plasma must revolve at a higher speed than the cold dense plasma.

Figure 1 presents a schematic to help visualize this point. The upper panel illustrates the perturbed magnetopause (MP) at the equatorial dawn flank that begins to roll over into a vortex by the KH instability. The magnetosheath flow is tailward ($V_x < 0$), while the magnetosphere is stagnant. Accordingly, across the boundary layer there is a velocity gradient. The drawing is shown in the frame of the vortex, so that the cold dense magnetosheath tongue (blue) protruding to the left is slowing down relative to the average flow, while the related hot tenuous magnetosphere protuberance (red) points to the right and accelerates toward the tail. The cold dense plasma intermingles with the hot tenuous plasma. The thick arrowed lines give an indication of the plasma motion. The thin blue lines are the conjectured deformation of the magnetosheath magnetic field projected into the XY plane. Hence (1) we expect an alternation of high and low density cycles in the data recorded by a spacecraft crossing the structure. Besides, (2) we anticipate that a scatter plot of V_x versus the plasma density N during the passage of the whirling flow should show the statistical trend indicated in the bottom panel. Features (1) and (2) are the basic elements of a criterion that permits the identification of a boundary roll-over in the observations.

Aside from (i) a case study addressing an interval of southward-pointing interplanetary magnetic field (IMF) [*Hwang et al.*, 2012a], and (ii) another study with a dawnward-pointing IMF [*Hwang et al.*, 2012b], most of the works on vortical structures at the magnetopause/boundary layer have concentrated on a strongly northward-pointing IMF, which is parallel to the Earth's field at low latitudes. If this lasts for several hours, it is typically associated with the northward-pointing phase of interplanetary magnetic clouds [*Burlaga et al.*, 1981]. A northward orientation favors a KH instability development because when the wave vector $\overrightarrow{k}$ of the perturbation is orthogonal to the average direction of the two magnetic fields ("*flute* " modes), or normal to the stronger one, the restraining magnetic forces are nearly canceled. At the same time, a substantial part of the velocity shear effect is retained. This argument applies equally well to southward IMF.

Here, by contrast, we focus on a situation where the IMF is oriented in a radial direction pointing approximately opposite to the solar wind flow. Under this configuration we present an example of rolled-up flow vortices making up the entire boundary layer at low latitudes a few R_E (Earth radii) tailward of the dawn terminator. The criterion for inferring the rolling-up stage, which was mentioned above, is satisfied. Furthermore, the Wind probe that recorded the rolling motion on October 24, 2001, was traveling orthogonal to the bulk motion of these structures, an ideal circumstance and one which is much superior to magnetopause-skimming orbits, which do not sample the whole structure of the vortices. In addition, the external field, too, was exceptionally steady and smooth in a plasma of low beta. In particular, there were no significant variations in the solar wind dynamic pressure. As noted by *Farrugia et al.* [2007] the magnetosphere was in a very quiescent state. Reconnection processes were at best weak and patchy (in time).

We then inquire into the possibility that the vortices are of KH origin. We adopt two approaches. In the first approach, we input parameters to the theoretical stability analysis taken from the exact MHD solution derived by *Spreiter and Rizzi* [1974] and appropriate for collinear field and flow. This theory was applied to the present event during the later time when Wind was crossing the magnetosheath [*Farrugia et al.*, 2010]. In the second approach we input to the theoretical calculations the observations made by the Wind spacecraft. In both cases we work with compressible MHD equations, using for the physical quantities continuous profiles across a thick boundary layer. This avoids pitfalls in the use of the stability condition for a thin boundary model (Appendix A, formula13), pointed out by *Gratton et al.* [2004a]. In both cases we find the region to be KH-unstable.

This is thus the first reported instance of rolled–up KH vortices populating a boundary layer under a near–radial IMF.

A magnetic field aligned with the flow is, of course, *prima facie* the most unfavorable configuration for the Kelvin-Helmholtz instability because the magnetic tension exerts a stabilizing action, which cannot be avoided by modes of the "*flute* " type. The stabilizing action of the field tension is precisely that avoided by "*flute* " modes. With a wave vector $\overrightarrow{k}$ perpendicular to the magnetic field, these eliminate its operation, but in field-aligned flows they eliminate also the instability driver. In this paper we discuss how, nonetheless, the configuration can be KH unstable.

A distinctive aspect of the case we present is that a radial magnetic field is forced to be drawn along by the billows when they arise. This constitutes a substantial difference from the KH instability for northward-pointing fields, where vortices can grow in a "*flute mode* " configuration, with only small changes in the orientation of the field lines.

The layout of the paper is as follows. After discussing the interplanetary data, we describe the observations in the boundary layer made by Wind. We then discuss elements of the KH instability relevant to our work. A summary and discussion follows. We give some technical details on the KH instability in the two appendices.

2. Observations

2.1. Interplanetary: ACE

Interplanetary conditions during the period we study consisted of a structure which formed the last in a set of interacting interplanetary coronal mass ejections (ICMEs). The ICMEs passed Earth during the five-day period from October 21 to October 25, 2001 (see *Farrugia et al.*, 2007) and were preceded by a strong shock. The state of the magnetosphere went from being strongly disturbed (October 21-October 23) to being almost quiescent. In the first period, two intense geomagnetic storms (Dst <-150 nT) were recorded. Then, on October 24-25, all organized activity subsided. This very quiet period ended when a trailing shock was seen advancing into the ICME sequence.

Observations over that part of this interval which is relevant to our study are shown in Figure 2. The interplanetary plasma and magnetic field observations are from the ACE spacecraft in orbit around the L1 Lagrangian point. They were acquired by the SWEPAM [*McComas et al.*, 1998] and MAG [*Smith et al.*, 1998] instruments, and are at 64 s (plasma) and 16 s (magnetic field) temporal resolution. The time interval shown is 18–21 UT, October 24, 2001. From top to bottom the panels display the proton density, temperature, (in red: the expected temperature after the statistical analysis of *Lopez*, 1987), bulk speed, the GSM components of the magnetic field (color-coded), the total field strength, the IMF cone angle, i.e. the angle made by the magnetic field to the Earth-Sun line, the dynamic pressure, the angle ('shear') between the field and flow vectors, the proton beta, and the sonic and Alfvén Mach numbers (M_s and M_A, respectively).

This period is marked by steady conditions and very smooth field and plasma temporal profiles. The temporal variations, which were a leading feature of the previous three days, have died down completely. The data show a slow (average and standard deviation: $\langle V \rangle = 372.5 \pm 2.5$ km s^{-1}) and very cold ($\langle T \rangle = 4187 \pm 375$ K) ICME, the proton temperature being about eight times less than the expected temperature. Compared to the normally dense slow solar wind, the density ($\langle N \rangle = 3.74 \pm 0.46$ cm^{-3}) is about one-half of a typical value of 7-10 cm^{-3}, leading to below-average dynamic pressure of 1.0 $\pm$ 0.10 nPa. As a consequence of this, the proton β is also very low, whence the smooth magnetic field profile. Because of the low T_p, the sonic Mach number M_s is very high, of order 35. At the position of Wind tailward of the dawn terminator, we therefore expect that effects due to compressibility of the plasma will be accentuated. The Alfvén Mach number is not particularly small ($\sim$7) and so the magnetic forces should not have a dominating influence on the instability. Importantly, the magnetic field has a near-radial orientation (panel 4) with a cone angle of $17.7° \pm 4.1°$. It makes an angle with the plasma flow vector of $162.0° \pm 4.7°$, so that it points almost opposite to the solar wind.

2.2. Observations in the dawnside boundary layer: Wind

In October 2001 the Wind spacecraft was orbiting the magnetosphere, reaching perigee in the near-geomagnetic tail region. Figure 3 shows its orbit from 19 UT, October 24 to 02 UT, October 25, after which time it exited into the solar wind [*Farrugia et al.*, 2010]. The red segments indicate the time when Wind was traversing the dawnside low-latitude boundary layer (LLBL) (19-20:30 UT, see below) downstream of the terminator at X $\sim$ -13.5 R_E and at somewhat northerly GSM latitudes (Z $\sim$ 5.5 R_E). This orbit cuts across any structures which are propagating downstream in this region. This is an ideal situation for our purposes.

Examples of the structures encountered in the period 19:00-19:30 UT are shown in Figure 4. The data are from the 3D Plasma Analyzer [3DP, *Lin et al.*, 1995] and the magnetic field investigation [*Lepping et al.*, 1995], both plotted at 3 s resolution. Shown from top to bottom are the proton density, bulk speed, temperature, the total field and its GSM components, and the GSM components of the flow vector. The dashed blue line in panel 2 gives the average magnetosheath velocity in the first half-hour after Wind's entry at 20:30 UT (= 314 km s^{-1}). The averages of the bulk flow velocity components are marked in the last three panels by the horizontal red lines. The average negative V_y-component (= -46 km s^{-1}) results from the dawnward flaring of the magnetopause (≈7.5°) at Wind's dawnside locale. Marked by vertical guidelines are the times when sharp increases in density occur and when simultaneously impulsive changes in the magnetic field and/or plasma parameters are evident. It should be noted that uncertainties in the plasma moment results do increase as the proton density drops below ∼0.1cm^{-3}. However, nowhere are the interpretation and conclusions of the paper affected by this.

We note the following features:

(i) Repetitive high-speed bursts of a hot tenuous plasma reaching speeds (up to ∼650 km s^{-1}) which are well in excess of the magnetosheath speed.

(ii) After the discontinuites (vertical lines), intervals of a cold dense (magnetosheath) plasma each lasting for ∼2-3 min are encountered.

(iii) In the Earth's frame, the cold dense plasma is moving more slowly tailward than the average flow. In the average velocity frame, its motion is thus predominantly sunward.

(iv) By contrast, in the average velocity frame the hot tenuous plasma is moving antisunward. Note the repeated overshoot of this plasma with respect to the antisunward velocity.

These last two points may be seen very well from the clear anti-correlated behavior of the density N and the antisunward velocity, -V_x.

(v) Sharp changes in the field and flow vectors, including abrupt polarity reversals, tend to occur at the leading edges of the cold dense (magnetosheath) structures. With one exception (that at 19:11 UT) the leading edges are thus simultaneously current and vortex sheets.

(vi) Considering only the largest changes (indicated by the vertical guidelines) there are six intervals of roughly repetitive structures with an average duration of ∼4.5 min. This average periodicity is retained throughout the entire 1.5 hr traversal of the LLBL, as we discuss below (section 2.3).

From (i) and (iv) we see that the criterion for identifying rolled-up vortices given in the Introduction, namely, a hot tenuous plasma flowing at speeds higher than that of the magnetosheath, is well satisfied. We now illustrate these features by focusing on one typical cycle of the plasma and field behavior.

Plasma and magnetic field data for a single cycle, corresponding to the interval marked by the horizontal red bar in the top panel of Figure 4, are shown in Figure 5. The same quantities as in Figure 4 are plotted in the first seven panels (note, however, the linear scale for the density). The last three panels show the plasma velocity in the average velocity frame. The approximate duration of the cycle is from ∼19:12:30 UT to ∼19:18:00 UT (∼ 5.5 min). The cold dense plasma interval is bracketed by the two vertical dashed red lines and lasts for ∼2:25 min. Immediately preceding the leading edge of the cold dense plasma at 19:12:20 UT, a plasma of low density and elevated temperature is moving at a speed exceeding that of the solar wind. The plasma there is flowing mainly perpendicular to the local magnetic field (not shown). The same may be seen from ∼19:16 to 19:18 UT ahead of the next cold dense plasma burst.

Relative to the average velocity, the cold dense plasma is moving mainly sunward ($\Delta V_x > 0$). With an average speed of 371 km s^{-1} and a duration of 2:25 min, the scale size of the cold dense plasma in the X-direction is estimated as 8.4 R_E. So it is very stretched in the X-direction, compared, say, to the distance around the magnetopause from the nose which is of order 20-25 R_E. After the cold dense plasma there follows a stage (∼19:15:10-19:16:00 UT) in which the plasma has acquired a dawnward velocity component ($\Delta V_y < 0$) and its sunward speed has decreased. Then comes a burst of hot tenuous plasma moving antisunward and northward and which ends up moving strongly antisunward and duskward. A rotational motion superposed on the antisunward and dawnward bulk flow is thus evident.

To visualize the flow rotation in the average velocity frame, we show in Figure 6 the residual flow vectors ΔV_x, ΔV_y for the period 19:12:30–19:18 UT. Time runs from the bottom to the top, and the labels 'S' and 'E' refer to the start and end of the interval. The arrows show the coordinates of the residual vectors. The blue arrows refer to the cold dense plasma, the red arrows to the hot tenuous plasma, and the green arrows to an intermediate state in (N, T). It is seen that, in the average velocity frame, the cold dense plasma is flowing mainly sunward with generally a very small duskward component (ΔV_y >0). The hot tenuous plasma (red) first flows tailward and then tailward and duskward. The flow direction of the plasma in between (green) starts rotating from a sunward and dawnward orientation and finishes in an antisunward orientation. This provides clear evidence of rolling-up (see Introduction).

2.3. General features of the Vortical Structures

The fact that the hot tenuous magnetospheric plasma is moving at speeds above those of the solar wind is strong evidence that the structure we are dealing with in Figure 6 is a rolled - up vortex [*Nakamura et al.*, 2004; *Takagi et al.*, 2006; *Hasegawa et al.*, 2004, 2006]. We wish now to confirm this for all the quasi-periodic structures seen by Wind in the interval 19:00-20:30 UT. In Figure 7 we plot in the bottom panel V_x versus N for the whole interval. The top panel show the same quantities for the one plasma and field cycle we have just been discussing. The color scheme indicates the temperature (red for hot and blue for cold). The dashed horizontal lines show the corresponding quantities when Wind entered the magnetosheath, (not shown; but see *Farrugia et al.*, 2010, their Figure 7), averaged over the first half-hour.

From the bottom panel it is seen that the bulk of the hot tenuous plasma is moving in an antisunward direction faster than the magnetosheath. Clearly also, the figure shows that the origin of the cold dense plasma is the magnetosheath. This is the same trend as seen in the single cycle plotted in the top panel although the highest speeds recorded there were ~ 580 km s^{-1}. Following *Takagi et al.* [2006], we conclude that Wind is observing an LLBL populated entirely by a sequence of rolled-up vortices.

Figure 8 depicts the motion of the plasma in the dawn-dusk direction in the form of a scatter plot of the residual ΔV_y versus ΔV_x for the whole interval 19:00–20:30 UT. The color is proportional to log T (red = hot) and the size of the squares to N. The figure shows a continuous distribution of ΔV_y values spanning across zero. There is no strong preference for positive or negative ΔV_y. The spread in ΔV_y of the hot tenuous plasma is wider. This overall picture confirms the persistence of the rotational motion in the average velocity frame quite clearly.

We recall from Figure 2 that interplanetary conditions were steady. Specifically, there were no significant variations in the dynamic pressure, P_{dyn}. But, in fact, there are large-amplitude, quasi-periodic fluctuations of this quantity generated by the vortices themselves. To show this, we consider in Figure 9 the temporal variation of P_{dyn} at Wind. The 1.5 - hour traversal is split into three ∼0.5-hour segments which are plotted underneath each another. Each panel shows the thermal plasma pressure (green trace) and the dynamic pressure (black trace). The blue and red traces are 21-point ($\sim$ 1 min) running averages of these two quantities, respectively. In computing the dynamic pressure, we took into account the average flaring of the dawn magnetopause, given by V_y in Figure 4. This gives a flaring angle of $\theta \approx 7.5°$ and the dynamic pressure has been multiplied by $sin(\theta)$. Underneath each plasma pressure panel, we plot the magnetic pressure for the corresponding interval. A linear scale is used for this.

One can see that the average dynamic pressure is subject to large-amplitude oscillations of period $\sim$5.0 min. Note that there are six clear waves corresponding to the vortices in the top panel. These are the ones identified in Figure 4 except for the small one between 19:11 and 19:12.2 UT, which might indicate some ongoing coalescence. The thermal plasma pressure behaves as the dynamic pressure, only at much reduced amplitude. The magnetic pressure is variable and its size is bigger than that of the plasma pressures. Overall pressure balance is not maintained. The fluctuations of the thermal pressure can produce ion acoustic waves along the geomagnetic field. The variation of the magnetic pressure can radiate magnetosonic waves across the magnetic field. The vortices can thus give rise to large scale effects in the plasma sheet.

3. Generating Mechanism: The Kelvin-Helmholtz Instability Source

The configuration of October 24, 2001 appears not to favor the onset of the KH instability: (i) the restraining magnetic forces are strong in field–aligned flows and (ii) the large M_s ushers in the other stabilizing factor, compressibility.

We now examine the issue more closely. We model the LLBL transition by continuous functions for the physical parameters. We call this "*thick model*" for short, to distinguish it from a "*thin*" approximation where the quantities suffer a discontinuous change across the boundary layer. (Appendix A, 13; see also *Gratton et al.*, [2004a], [2004b]; *Gnavi et al.*, [2009]). For the stability analysis we work in a flow-aligned coordinate system defined as follows. The x-axis points in the direction of the local $\overrightarrow{V}$. The y-axis points across the LLBL, normal to the local magnetopause and directed outward. The z-axis completes the right-handed Cartesian triad, and is oriented in the same sense as geomagnetic north.

Scalar and vector quantities in the LLBL are represented by hyperbolic tangent functions with a scale length d, for example:

$$V_x = V_1(1 + \tanh(y/d))/2, \tag{1}$$

for the velocity, and with similar expressions for $\overrightarrow{B}$ and N (Appendix A). Subscripts '1' and '2' refer to magnetosheath and magnetosphere quantities, respectively. The temperature profile $T(y)$ follows from the pressure balance equation across the layer (Appendix B). We take $D = 4d$ as a representative value for the LLBL thickness, which ranges approximately from $y = -2d$ to $+2d$. The normalized quantities contain d and V_1 implicitly such as, for example, in the normalized growth rate $g = \gamma d/V_1$. An estimated value of D, and a measured value of V_1, can be introduced in the discussion at the end of the theoretical calculation; it is not necessary to assume them beforehand. The compressible MHD stability theory used here is summarized in Appendix A, where some details of the procedure can be found. For every k-mode the KH instability is driven by the intensity of the velocity projection V_k in the $\overrightarrow{k}$-direction ($V_k = \overrightarrow{V} \cdot \widehat{k}$, where $\widehat{k} = \overrightarrow{k}/|\overrightarrow{k}|$). The magnetic tension that opposes the instability depends on the magnetic field projection B_k in the $\overrightarrow{k}$ -direction ($B_k = \overrightarrow{B} \cdot \widehat{k}$).

We follow two approaches regarding the physical parameters which we input into the theory. In the first approach, the Mach numbers are based on the *Spreiter and Rizzi* [1974] theory, that gives an approximate representation of the solar wind – magnetosheath transition for collinear MHD flows. We use the Spreiter – Rizzi solution with solar wind input from ACE. Close to the terminator this theory predicts approximately: $M_s = 7.7$, $M_A = 4.9$, which corresponds to a magnetosheath plasma $\beta_1 = 0.97$.

The geomagnetic field on the dayside is assumed to be perpendicular to $\overrightarrow{V}$, i.e. the magnetic shear angle in this model is 90°. Presumably, this angle was not exactly 90°, and it varies with the distance from the subsolar point. But we think that near Earth deviations from 90° could not have been substantial. Anyway, the chosen shear angle is not critical to decide on the instability because we intend to switch-off – or, at least, much reduce – the magnetic tensions on the magnetosphere side of the LLBL by considering k -vectors normal to the local geomagnetic field. This choice of $\overrightarrow{k}$ favors V_k, the driver of the instability (and maximizes it when the magnetic shear angle is exactly 90°), but exposes the k -mode to the full stabilizing influence of the magnetosheath field projection B_k. For the dayside we assume a typical particle density ratio $N_2/N_1 \sim 0.1$.

The pressure balance equation imposes an upper limit on the magnetic field ratio $B_2/B_1 < 1.4$. (About this requirement see condition 20 in Appendix B.) In approach (1) we computed with $B_2/B_1 = 1$, $n_2/n_1 = 0.1$, and (as a consequence of eq.(19), Appendix B) a temperature ratio $T_2/T_1 \sim 10$. The choice reflects expected values at the MP away from the subsolar point, but still near Earth, as the terminator.

The mode considered is with $\overrightarrow{k}$ parallel to the flow. (Computation shows it to be the $\overrightarrow{k}$ orientation of fastest growth.) Figure 10 shows the (normalized) imaginary part of the characteristic value, $c_i = \gamma/kV_1$, as a function of kd. Quantity c_i is a linear function of kd in most of the interval (for $kd \geq 0.15$), so that the growth rate $g = \gamma d/V_1$ as a function of kd is approximated by a parabola (not shown). The maximum of the normalized growth rate $g = c_i kd = \gamma d/V_1$ occurs at kd =0.245 (λ =6.41D) for g =0.0832. From this value we may estimate an e-folding time $\tau_e = 1/\gamma \sim 48$ s for LLBL sites near the terminator, with $D = 0.5R_E$, assuming that the LLBL thickness is not yet broadened by the instability, and with $V_1 \sim 200$ km/s. Therefore, in a boundary layer not yet widened by perturbations, the KH instability can grow quite fast. We think that the vortices observed by Wind are generated in the LLBL closer to Earth.

We now discuss the second approach. Here we input to the model data acquired during the Wind's LLBL traversal. The scenario is a composition of averages of measurements: (a) made in the magnetosphere before, but close to, the entrance to the LLBL (including early times of the passage through it) with (b) data recorded – albeit later – in the adjacent magnetosheath.

At Wind's position, with a magnetosheath average velocity of 314 km s^{-1} , the Mach numbers computed with data for that region are $M_s = 5.6$ and $M_A = 6.8$. They lead to a plasma of $\beta_1 = 3.5$. The magnetic field $\overrightarrow{B}$ in the magnetosheath is still approximately collinear with the flow [*Farrugia et al.*, 2010]. A difference from approach 1 is that the magnetic shear angle is not 90° (as hypothesized for near-Earth positions) but 71° with respect to the sunward direction (taken from an average $\overrightarrow{B}$ on the magnetosphere side).

To sum up, the input parameters for the stability analysis are as follows.

Table 1

Magnetosheath	Magnetosphere
$M_s = 5.6,\ M_A = 6.8$	$-----------$
$V_1 = 314$ km/s	$V_2 = 0$
$N_1 = 5$ cm^{-3}	$N_2 = 0.05$ cm^{-3}
$B_1 = 4.5$ nT	$B_2 = 9.5$ nT
$\chi_1 = 180°$	$\chi_2 = 109°$

where χ denotes the angle that the magnetic field makes with the x-axis. Inside the magnetosphere the total pressure is almost purely magnetic, but in the magnetosheath thermal and magnetic pressures are of the same order. The B_2/B_1 ratio satisfies condition (20) Appendix B close to the limiting value 2.13, but the quantities still conform to an approximate pressure balance across the BL (the upper bound of 20 could be a bit larger with a correction for flaring).

Figure 11 shows the normalized growth rate g a function of kd. It reaches a still significant maximum value $g = 0.033$ at $kd = 0.43$ and goes to zero at $kd \approx 0.07$ (long λ) and $kd = 0.84$ (short λ). The angle of $\overrightarrow{k}$ with the x axis is ϕ =19 °. With a ratio $N_2/N_1 = 10^{-2}$ the growth rate γ is zero in the $kd \rightarrow 0$ limit. This is a case of stability at long wavelengths.

The second approach intends to show that a steady-state LLBL model, endowed with equilibrium quantities represented by continuous functions that connect mean values of magnetospheric and magnetosheath data, is unstable. The averages include long stretches of time on either side of the LLBL, because the instability is found with wavelengths of several R_E, and the penetration depth of the KH perturbation is expected to be large. However, the LLBL and the magnetosheath are both perturbed already. The former by the passage of vortical structures as discussed in section 2, which we conclude are formed at some place near Earth; the latter by the turbulence after the bow shock, and by large amplitude oscillations of long period [*Farrugia et al.*, 2010]. Nonetheless the result is an indication that the LLBL, at the Wind's orbit position, has amplifying properties regarding the KH instability mechanism. In other words, if by reason of intermittency the passage of vortical perturbations is temporarily suspended, the (unstable) background LLBL still maintains the capability to grow perturbations, and eventually to roll-over the velocity gradient layer again.

4. Summary and Discussion

We took advantage a rare coincidence of a long interval of radial IMF, steady solar wind conditions, and a spacecraft taking observations along a path that cuts perpendicularly through the near-Earth flank of the magnetosphere. The Wind observations through the LLBL at X=-13 Re showed the LLBL to be full of rolled-up vortices. These were shown to arise from the KH instability. The new result here is not so much the observation of KH-like oscillations but that they occur under a radial IMF, which should suppress the growth of KH waves. So, while rolled-up vortices for northward IMF have been reported before, this is first reported case of observations of KH rolled-up vortices for radial IMF.

In some ways this was a continuation of work started in *Farrugia et al.*, [2007], [2010]. In those papers we focussed on the extremely quiet state of the magnetosphere after a three-day long period of strong disturbance. The cause was a series of ICMEs, and the period we concentrated on here constituted the last of these where very steady conditions prevailed. The *Farrugia et al.* [2010] study of this event dealt with the entire magnetosheath showing that the near-parallel alignment of field and flow held throughout the magnetosheath and that the data matched a relevant theory that treats flow-aligned field in the magnetosheath.

In a 1.5 hr traversal we identified approximately 15 vortices. We argued they had reached the non-linear stage and had started to roll up. The rolling-up process was inferred from the repeated presence of a low density, magnetosphere plasma moving antisunward at speeds greater than in the magnetosheath, which recent studies have shown to be a reliable indicator of such structures based on single-spacecraft *in situ* observations.

We then presented two KH instability calculations using different inputs for the theory model of the transitions In the first we inputted data from the theory of *Spreiter and Rizzi* [1974], which gives an exact MHD solution for field-aligned flows. In the second, we inputted direct measurements made by Wind in the magnetosphere and in the magnetosphere at the beginning and end of the LLBL crossing, respectively. In both cases the LLBL was found to be unstable.

Although the solar wind dynamic pressure was very steady, the passage of the structures gave rise to large-amplitude modulations of the magnetic pressure and the dynamic pressure in the boundary layer. This could set up waves travelling along (ion acoustic waves) and perpendicular (magnetosonic waves) to the magnetic field. This shows that the passage of the large vortices at dawn could influence large parts of the plasma sheet.

We now discuss various aspects of the observations of the October 24, 2001 event. In previous work, *Farrugia et al.* [2007] concentrated on the very low level of geomagnetic disturbances which prevailed on this day. Such were, for example, an average Kp index = 0+, polar caps which had very weak electron precipitation without any consistent north-south asymmetries, and patchy and weak reconnection at low latitudes or poleward of the cusp. In particular, the authors noted a cross-polar cap potential of ∼20 kV. This would be of about the same magnitude as that commonly ascribed to the contribution to the

CPCP of viscous-type interactions. However, *Farrugia et al.* [2007] argued against the KH instability. This conclusion was essentially based on the lack of ULF pulsations of the geomagnetic field in the Pc 5 range (2-7 mHz), which the KH instability is often thought to give rise to via the field line resonance theory [*Chen and Hasegawa*, 1974; *Southwood*, 1974]. They thus could not find a solar wind driver for the weak and patchy convection.

Was the instability a result of the (radial) direction of the IMF, or was it favored by specific values of the Mach numbers in this case? This is an important question that deserves further attention. We think that in this case M_A values (estimated at the terminator, and measured at Wind's orbit) were clearly helping the onset, and development of the instability. The radial field orientation is unfavorable, in general, to the KH instability. However, even in the case of normal solar wind and Parker's spiral field, there is the possibility that KH waves may develop inside the boundary layer, and grow thereafter tailwards. Further work is necessary to test other cases to see if it was the radial IMF orientation that did this, or rather other favorable parameters.

From the theory it was concluded that (i) in both approaches the boundary of this wide LLBL was KH unstable and (ii) the long wavelength limit is stable. That is, a thin layer would be stable. The instability appears only with the thick boundary layer. We also concluded that the generating site was well upstream of the observation locale. As a consequence of the stability study, we assume, as seems reasonable, that the lifetime of each member of the vortex sequence is similar because they are generated approximately at the same position upstream (closer to the Earth).

If a magnetic field collinear with the flow is generally unfavorable to the development of the KH instability, and the magnetosheath motion was supersonic, why is the LLBL unstable in this event? This is so because the physical conditions of the inner edge of the LLBL are very different from those of the outer edge (adjacent to the magnetosheath). That the inner edge of the LLBL, in general, may be prone to the KH instability was also considered by other authors, among them *Ogilvie and Fitzenreiter*, [1989], and *Miura*, [1992].

Behind the bow shock, the magnetosheath is frequently in a turbulent state. The plasma of the boundary layer is pulled along by the solar wind. A velocity shear flow parallel to that of the magnetosheath is established across this layer. The motion is subsonic inside the LLBL, because of the decreased speed with respect to the magnetosheath, and the higher temperature of the magnetospheric plasma. At the equatorial dayside, the geomagnetic field is mainly normal to the flow. At the inner edge side, even if moving at reduced speed, the obstacles to the growth of the KH instability are attenuated. Flute modes with a wave vector normal to the local geomagnetic field, and parallel to the internal flow direction, are not restrained by magnetic tension forces, and the low compressibility reduces additional stabilizing effects. Downstream, M_A increases and magnetic tensions are further reduced, so that conditions for instability improve.

A major reason why people are interested in the non-linear stage of the KH instability in the first place is that, by breaking the frozen-in condition, it offers the possibility for mass transfer. This transfer would happen at current sheets where oppositely-directed magnetic fields have been brought next to each other during the rolling-up process (see Figure 4). We found several instances of current and vortex sheets. Indeed, most field and flow cycles contained one of these.

Current sheets are prone to magnetic line tearing, and hence are a possible way to mass transport across the MP (see e.g. *Otto and Fairfield*, [2000], and *Otto and Nykyri*, [2003] for computer simulation studies of field lines coiled-up inside vortices). From the data we cannot tell to what extent the field lines are entrained by the vortices. But we find repeated evidence of current sheet formation. Whether mass transport is actually taking place in our case will be pursued in a further study.

Our work and that of *Hwang et al.* [2012a], [2012b] show that it is not necessary to have a northward-pointing IMF to excite the KH instability. Neither is it necessary for the IMF to point north to produce field configurations conducive to reconnection and, by implication, mass entry.

5. Appendix A. KH Theory

The LLBL model with continuous functions used in section 3 describes a MHD parallel flow with a local x axis directed along the velocity field. (The flow does not change direction.) The physical quantities are constant over (x, z) planes, and vary only in the transverse y direction, chosen to be normal to the MP. However, in general, the magnetic field may change both in direction and strength. The unperturbed (or average state) LLBL model is given by a set of functions: $\overrightarrow{V} = (V_x(y), 0, 0)$, $\overrightarrow{B} = (B_x(y), 0, B_z(y))$, $\rho(y) = m_p N(y)$, for velocity, magnetic fields, and mass density ρ or particle density N, respectively. The temperature function $T(y)$ results from this set of functions and the pressure balance equation (Appendix B).

Across the LLBL, the physical quantities have hyperbolic function profiles:

$$V_x = V_1(1 + \tanh(y/d))/2, \tag{2}$$

$$B = (B_1 + B_2)/2 + (B_1 - B_2)\tanh(y/d)/2 \tag{3}$$

$$\theta = (\theta_1 + \theta_2)/2 + (\theta_1 - \theta_2)\tanh(y/d)/2 \tag{4}$$

$$B_x = B\cos(\theta), \quad B_z = B\sin(\theta) \tag{5}$$

$$N = (N_1 + N_2)/2 + (N_1 - N_2)\tanh(y/d)/2 \tag{6}$$

where d is a scale length. The width D of the thick LLBL model is taken as $D = 4d$.

The perturbation modes of the KH instability are of the form

$$\Xi = \zeta(y)\exp(-i\omega t + ik_x x + ik_z z), \tag{7}$$

where Ξ is the y-component of the Lagrangian displacement of a plasma element from a steady state position, and $\zeta(y)$ is the corresponding amplitude. The (complex) angular frequency of the modes is denoted by $\omega = \omega_r + i\gamma$. The real part ω_r gives the frequency of the oscillations, and the imaginary part is the growth rate of the instability when $\gamma > 0$; the e-folding time is $\tau_e = 1/\gamma$. The wavevector is represented by $\overrightarrow{k} = (k_x, 0, k_z)$, $k = |\overrightarrow{k}|$ is the wavenumber; $\lambda = 2\pi/k$ is the wavelength.

The amplitude of the Fourier modes of the KH perturbation is governed by the second order differential equation,

$$\frac{d}{dy}\left[H\left(1 - \frac{1}{M}\right)\frac{d\zeta}{dy}\right] - k^2 H\zeta = 0, \tag{8}$$

derived from the linearized equations of ideal (non–resistive), compressible MHD [*Gratton et al.*, 1988]. A complex phase velocity $c = \omega/k$ is introduced so that the functions $H(y)$ and $M(y)$ of the differential equation for ζ can be written as,

$$H(y) = \rho\left[(c - V_k)^2 - V_{Ak}^2\right], \tag{9}$$

$$M = 1 - \frac{c_s^2 + V_A^2}{(c - V_k)^2} + \frac{c_s^2 V_{Ak}^2}{(c - V_k)^4} \tag{10}$$

where $V_A = B/\sqrt{4\pi\rho}$ is the Alfvén speed, $V_{Ak} = B_k/\sqrt{4\pi\rho}$, is a projected Alfvén speed, c_s is the speed of sound, and V_k, B_k are projections of the velocity and magnetic fields in the $\overrightarrow{k}$ direction. All these quantities are functions of y. The analysis is of a temporal type, that is, a (real) wavenumber $\overrightarrow{k}$ is given (as a Fourier component of the initial perturbation), and the response of the system determines the unknown (complex) value of c. To obtain c a boundary value problem for equation 8 must be solved.

When $c_s \to \infty$, the coefficient $M \to \infty$, and equation (8) reduces to

$$\frac{d}{dy}\left[H\frac{d\zeta}{dy}\right] - k^2 H\zeta = 0, \tag{11}$$

that represents the incompressible MHD approximation. When the transition layer is very thin with respect to the wavelength, that is when $kd \ll 1$, an approximate dispersion relation can be derived:

$$H_1 + H_2 = 0, \tag{12}$$

where H_1 and H_2, are the values taken by H on each side of the BL; labels 1 and 2 refer to the magnetosheath and magnetosphere, respectively. This is the"*thin model*" result for incompressible plasma flows. From equation (12) a well known stability condition follows,

$$\rho_R \left(\Delta\overrightarrow{V} \cdot \widehat{k}\right)^2 \leq \frac{1}{4\pi}\left[\left(\overrightarrow{B_1} \cdot \widehat{k}\right)^2 + \left(\overrightarrow{B_2} \cdot \widehat{k}\right)^2\right]. \tag{13}$$

where ρ_R is defined by $1/\rho_R = (1/\rho_1 + 1/\rho_2)$, and $\Delta\overrightarrow{V} \equiv V_1 - V_2$. The "*thin model*" condition, often used in the current literature, ensures stability when it holds for all directions of $\overrightarrow{k}$. The thin model stability does not depend on the wavelength.

The intricacy of the boundary value problem for equation (8) with finite wavelengths derives from the fact that c is not an eigenvalue but a characteristic value entangled in a non-linear fashion in the functions H and M. Moreover, when the direction of $\overrightarrow{k}$ changes, the functions $V_k(y)$, $B_k(y)$ (and other functions, such as $c_s(y)$, etc.) also change. Thus the analysis requires the solution of separate differential equations for every $\overrightarrow{k}$ direction. In this paper we solved the boundary value problem for c using a conventional shooting method. The compact form of equation (8) facilitates the use of shooting methods.

6. Appendix B. Pressure Balance Condition

The field functions of the local LLBL model, $B(y), \rho(y), T(y)$, etc., must satisfy pressure balance,

$$p_1 + \frac{B_1^2}{8\pi} = p(y) + \frac{B(y)^2}{8\pi} = p_2 + \frac{B_2^2}{8\pi}. \tag{14}$$

Here $p = nk_B(T_i + T_e)$ is the thermal pressure (k_B is Boltzmann's constant). We assume a common temperature value $T_i = T_e = T$ (in our case the proton temperature is from spacecraft data).

It is convenient to write equation (14) in terms of M_s and M_A, both computed with magnetosheath parameters adjacent to the local LLBL. Quantity $M_s = V_1/c_{s1}$, where $c_{s1} = \sqrt{(\gamma k_B T_e/m_i)} = \sqrt{(\gamma k_B T_1/m_p)}$ ($\gamma = 5/3$, and $m_i = m_p$ is the proton mass). Similarly, $M_A = V_1/V_{A1}$, with $V_{A1} = B_1/\sqrt{4\pi\rho_1} = B_1/\sqrt{4\pi n_1 m_p}$. Then eq. 14 can be written in the form

$$\frac{1}{\rho_1 V_1^2}\left[p(y) + \frac{B(y)^2}{8\pi}\right] = \frac{\rho}{\rho_1 V_1^2}\left(\frac{4}{\gamma}c_s^2(y) + V_A^2(y)\right) = \left(\frac{4}{\gamma}\frac{1}{M_s^2} + \frac{1}{M_A^2}\right). \tag{15}$$

When M_s and M_A are known, the plasma beta is fixed because

$$\beta = \frac{2nk_BT}{B^2/8\pi} = \frac{4}{\gamma}\frac{c_s^2}{V_A^2}, \tag{16}$$

and since we are interested in the magnetosheath beta,

$$\beta_1 = \frac{4}{\gamma}\frac{M_A^2}{M_s^2}. \tag{17}$$

From these, the temperature function across the boundary layer can be written as,

$$\frac{T(y)}{T_1} = \frac{n_1}{n(y)} \left[1 + \frac{1}{\beta_1} \left(1 - \frac{B(y)^2}{B_1^2} \right) \right]. \tag{18}$$

The local magnetosphere-to-magnetosheath temperature ratio is therefore:

$$\frac{T_2}{T_1} = \frac{n_1}{n_2} \left[1 + \frac{1}{\beta_1} \left(1 - \frac{B_2^2}{B_1^2} \right) \right], \tag{19}$$

which implies that the magnetosheath beta, β_1, together with the magnetic field intensity ratio B_2^2/B_1^2, set a limit to the steady state boundary layer models. A local pressure balance does exists when

$$B_2^2/B_1^2 < 1 + \beta_1, \tag{20}$$

and we see that T_2 becomes zero when $B_2^2/B_1^2 = 1 + \beta_1$. Under ordinary conditions, the magnetosheath β_1 is much larger than unity, so that this limitation is not important. But in the October 24, 2001 event the values of β_1 are comparable to, or even smaller than, unity. Hence, when setting stability models the constraint (20) must be taken into account.

Condition (20) needs a correction when the boundary is flared with respect to the solar wind flow due to the presence of a normal component of the momentum flux. In practice, this can be approximately assumed as an increment of the effective B_1^2, and then (20) becomes a less severe bound.

7. Acknowledgments

We thank the referees for their many helpful comments. We thank all the providers of the data used here: Adam Szabo for the Wind magnetic field data; Dave McComas and Charles Smith for the ACE plasma and field data through NASA's cdaweb site. FTG and

GG are grateful for the support of the Argentine CONICET, grant 11220090100608 PIP 2010 - 2012. This work is supported by NASA grants NNX10AQ29G and NNX13AP39G.

References

Burlaga, L. F., Sittler, E., Mariani, F., and Schwenn, R. (1981), Magnetic loop behind an interplanetary shock: Voyager, Helios and IMP 8 observations, *J. Geophys. Res., 86,* 6673.

Chen, L., and A. Hasegawa (1974), A theory of long–period magnetic pulsations, 1. Steady state excitation of field line resonance, *J. Geophys. Res., 79(7)*, 1024.

Chen, S. -H., and M. G. Kivelson (1993), On nonsinusoidal waves at the Earth's magnetopause, *Geophys. Res. Lett., 20(23)*, 2699, doi:10.1029/93GL02622.

Cowley, S. W. H. (1982), The causes of convection in the Earth's magnetosphere: A review of developments during the IMS, *Rev. Geophys., 20*, 531.

Farrugia, C. J., F. T. Gratton, and R. B. Torbert (2001), The role of viscous-type processes in solar wind-magnetosphere interactions, in Challenges to long-standing unsolved problems in space physics in the 20th century, *Space Science Rev.*, 95, 443.

Farrugia, C. J., A. Grocott, P. E. Sandholt, S. W. H. Cowley, Y. Miyoshi, F. J. Rich, V. K. Jordanova, R. B. Torbert, and A. Sharma (2007), The magnetosphere under weak solar wind forcing, *Ann. Geophys., 25*, 1.

Farrugia, C. J., N. V. Erkaev, R. B. Torbert, H. K. Biernat, F. T. Gratton. A. Szabo, H. Kucharek, H. Matsui, R. P. Lin, K. W. Ogilvie, R. P. Lepping. C. W. Smith (2010), Magnetosheath for almost-aligned solar wind magnetic field and flow vectors: Wind observations across the dawnside magnetosheath at X = -12 R_E *J. Geophys. Res. 115,* A08227, doi:10.1029/2009JA015128.

Gnavi, G., F. T. Gratton, C. J. Farrugia and L. E. Bilbao (2009), Supersonic mixing layers: stability of magnetospheric flanks models. *Journal of Physics: C. S.* **166** 012022, doi:10.1088/1742-6596/166/1/012022.

Gratton, F. T., L. Bender, C. J. Farrugia, and G. Gnavi (2004a), Concerning a problem of the Kelvin-Helmholtz instability of the thin magnetopause, *J. Geophys. Res.* A **109** doi: 10.102 V2003JA010146.

Gratton, F. T., G. Gnavi, C. J. Farrugia, and L. Bender (2004b), On the MHD boundary of Kelvin-Helmholtz stability diagrams at large wavelengths, *Brazilian J. Phys.* **34** 1804-1813.

Gratton J., F. T. Gratton, and A. G. González (1988), Convective instability of internal modes in accelerated compressible plasmas, *Plasma Phys. Contr. Fusion* **30** 435-456.

Hasegawa, H., M. Fujimoto, K. Takagi, Y. Saito, T. Mukai, and H. Rème (2006), Single–spacecraft detection of rolled–up Kelvin-Helmholtz vortices at the flank magnetopause, *J. Geophys. Res., 111, A09203*, doi:10.1029/2006JA011728.

Hasegawa, H., M. Fujimoto, T.-D. Phan, H. Rème, A. Balogh, M. W. Dunlop, C. Hashimoto, and R. TanDokoro (2004), Transport of solar wind into Earth's magnetosphere through rolled-up Kelvin-Hemholtz vortices, *Nature, 430*, 755.

Hwang, K.-J., M. M. Kuznetsova, F. Sahraoui, M. L. Goldstein, E. Lee, and G. K. Parks (2012a), Kelvin-Helmholtz waves under southward interplanetary magnetic field, *J. Geophys. Res., 116*, A08210, doi:10.1029/2011JA016596.

Hwang, K.-J., M. L. Goldstein, M. M. Kuznetsova, Y. Yang, and A. Viñas (2012b), The first in situ observation of Kelvin-Helmholtz waves at high latitude magnetopause during strongly dawnward interplanetary magnetic field conditions (2012), *J. Geophys. Res., 117*, A08233, doi:10.1029/2011JA017256.

Lepping, R., and L. Burlaga (1979), Geomagnetopause surface fluctuations observed by Voyager 1, *J. Geophys. Res., 84(A12)*, 7099-7106.

Lepping, R. P., et al. (1995), The Wind Magnetic Field Investigation, *Space Sci. Rev., 71*, 207.

Lin, R. P., et al. (1995), A Three-Dimensional Plasma and Energetic Particle Investigation for the Wind spacecraft, *Space Sci. Rev., 71*, 125.

Lopez, R. E. (1987), Solar cycle invariance in solar wind proton temperature relationships, *J. Geophys. Res., 92,* 11,187.

Miura, A. (1992), Kelvin-Helmholtz instability at the magnetospheric boundary: Dependence on sonic Mach number, *J. Geophys. Res., 97*, 10655.

McComas, D. J., et al. (1998), Solar wind electron proton alpha monitor (SWEPAM) for the advanced composition explorer, *Space Sci. Rev., 86,* 563.

Nakamura R., W. Baumjohann, T. Nagai, M. Fujimoto, T. Mukai, B. Klecker, R. Treumann, A. Balogh, H. Rème, J. A. Sauvaud, L. Kistler, C. Mouikis, C. J. Owen, A. N. Fazakerley, J. P. Dewhurst and Y. Bogdanova (2004), Flow shear near the boundary of the plasma sheet observed by Cluster and Geotail, *J. Geophys. Res., 109, A18*, 5204, doi:10.1029/2003JA010174.

Ogilvie, K. W., and R. J. Fitzenreiter (1989), The Kelvin-Helmholtz Instability at the Magnetopause and Inner Boundary Layer Surface, *J. Geophys. Res., 94 (A11)*, 15, 113, 123.

Otto, A., and D. Fairfield (2000), Kelvin-Helmholtz instability at the magnetotail boundary: MHD simulation and comparison with Geotail observations, *J. Geophys. Res., 105(A9)*, 21175.

Otto, A. and K. Nykyri (2003), Earth's Low-Latitude Boundary Layer Magnetopause *Geophys. Monog. Ser. vol 133* ed. P. T. Newell and T. Onsager (Washington DC: AGU), 53.

Sckopke, N., G. Paschmann, G. Haerendel, B. Sonnerup, S. Bame, T. Forbes, E. Hones, and C. Russell (1981), Structure of the low-latitude boundary layer, *J. Geophys. Res., 86, A4*, doi:10.1029/JA086iA04p02099.

Smets R., D. Delcourt, G. Chanteur, and T. E. Moore (2002), On the incidence of Kelvin-Helmholtz instability for mass exchange process at the Earth's magnetopause, *Ann. Geophys. 20*, 757.

Smith, C. W., J. L'heureux, N. F. Ness, M. H. Acuna, L. F. Burlaga, and J. Scheifele (1998), The ACE magnetic fields experiment, *Space Sci. Rev., 86,* 613.

Southwood, D. J. (1974), Some features of field line resonances in the magnetosphere, *Planetary and Space Science, 22, Issue 3*, p. 483-491.

Spreiter, J. R., and A. W. Rizzi (1974), Aligned magnetohydrodynamic solution for solar wind flow past the earth´s magnetosphere, *Acta Astron.*, **1**, 15, 1974.

Takagi, K., C. Hashimoto, H. Hasegawa, M. Fujimoto, and R. TanDokoro (2006), Kelvin-Helmholtz instability in a magnetotail flanklike geometry: Three-dimensional MHD simulations, *J. Geophys. Res., 111, A08202*, doi:10.1029/2006JA011631.

8. Figure Captions

Figure 1

A schematic to help interpret the Wind data. The wavy magnetopause at the equatorial dawn flank is shown in the top panel as it begins to roll over into a vortex by the KH instability. The magnetosheath flow is tailward ($V_x < 0$), while the magnetosphere is stagnant. The drawing is shown in the frame of the vortex, so that the cold dense magnetosheath tongue (blue) protruding to the left is slowing down relative to the average flow, while the related hot tenuous magnetosphere is moving faster. The bottom panel shows expectations drawn from this for the scatter plot of V_x versus N.

Figure 2. ACE plasma and field observations during 18-21 UT, October 24, 2001. The panels show the proton density, temperature (in red: the expected temperature for normal solar wind expansion), bulk speed, the total field and (colored) its GSM components, the IMF cone angle, the dynamic pressure based on the protons, the angle between the field and flow vectors, the proton beta, and the sonic and Alfvén Mach numbers.

Figure 3. A segment of Wind's orbit for the time interval 19 UT, October 24–02 UT, October 25. The plot shows the trajectory projected into the X-Y and X-Z planes. Tick marks are shown at each hour. The red segment (19:00 - 21:30 UT) refers to the time Wind was crossing the LLBL, thus moving predominantly dawnward.

Figure 4. Proton plasma and magnetic field observations from Wind for the period 19:00-19:30 UT. From top to bottom: the proton density, bulk speed, temperature, the total field and its GSM components, and the GSM velocity components. The dashed blue line in panel 2 gives the average magnetosheath speed. Dashed red lines in last three panels show the average values

of the respective quantities over the interval plotted. Note the speeds of the hot tenuous plasma, which exceed the solar wind.

Figure 5. Wind plasma and field data for the time interval ∼19:12 UT to ∼19:18 UT. The format is the same as for Figure 4, except that the last three panels show the velocity components in the average velocity frame, i.e. when the average velocity computed over this interval is subtracted.

Figure 6.

Residual vectors in the XY plane for the structure in Figure 5. Symbols S and E mark the start and end of the structure. The labels CD and HT refer to "cold dense" and "hot tenuous", respectively. Time runs from bottom to top. The blue, green, and red vectors represent differing plasma parameters, as explained in the text. In the average velocity frame shown, the flows start moving sunward and slightly duskward (blue). They then rotate dawnward and become progressively antisunward (green), and finish flowing antisunward and duskward (red).

Figure 7.

Scatter plots of V_x versus N for the vortex at 19:12:30–19:18:00 UT (upper panel) and for the whole LLBL crossing (lower panel). The logarithm of the temperature is indicated by the colors, where red = hot and blue = cold. Velocities are plotted in the Earth's frame. The horizontal dashed line marks the average magnetosheath speed observed when Wind crossed into this region at 20:30 UT (not shown; see *Farrugia et al.*, 2010; their Figure 7). Both panels show the presence of (i) a hot tenuous plasma moving at high speeds tailward and (ii) a dense cold plasma moving antisunward at speeds close to that of the magnetosheath. The figure shows clearly that the origin of the cold dense plasma is the magnetosheath.

Figure 8

The figure shows a scatter plot of ΔV_y against ΔV_x for the whole interval. Color is proportional to log T and size is proportional to N. The plot is in the average velocity frame. The distribution in the dawn-dusk direction ΔV_y shows a wide spread across zero. It is wider for the hot tenuous plasma.

Figure 9 For three sub-intervals, the plot shows pairwise the proton thermal pressure and dynamic pressure and below the magnetic pressure. The smoothed average of the thermal and dynamic pressure are shown by a blue and red traces, respectively.

Figure 10

Normalized imaginary part of c, i.e., the complex phase velocity γ/kV_1, versus kd. Hyperbolic tangent model with input parameters from the Spreiter-Rizzi theory [1974] for a boundary layer at the terminator. Quantities $M_s = 7.7$, $M_A = 4.9$.

Figure 11

Normalized growth rate as a function of kd. The input parameters for the stability calculations are based on Wind data. Maximum growth rate is reached at $kd = 0.43$. For further details, see text.

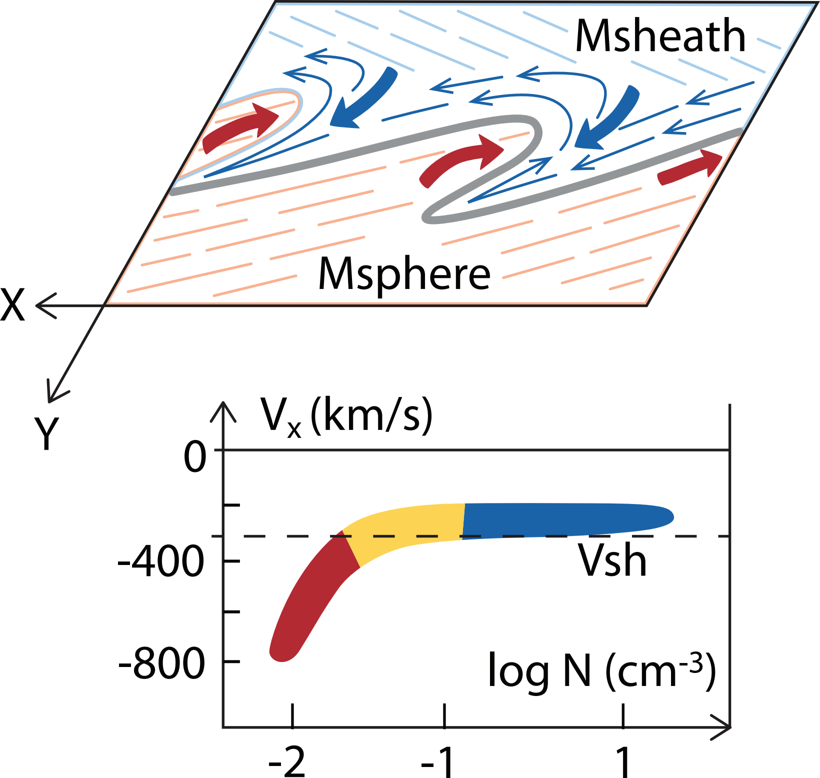

Msheath
Msphere
X
Y
Vx (km/s)
0
-400
-800
Vsh
log N (cm-3)
-2
-1
1

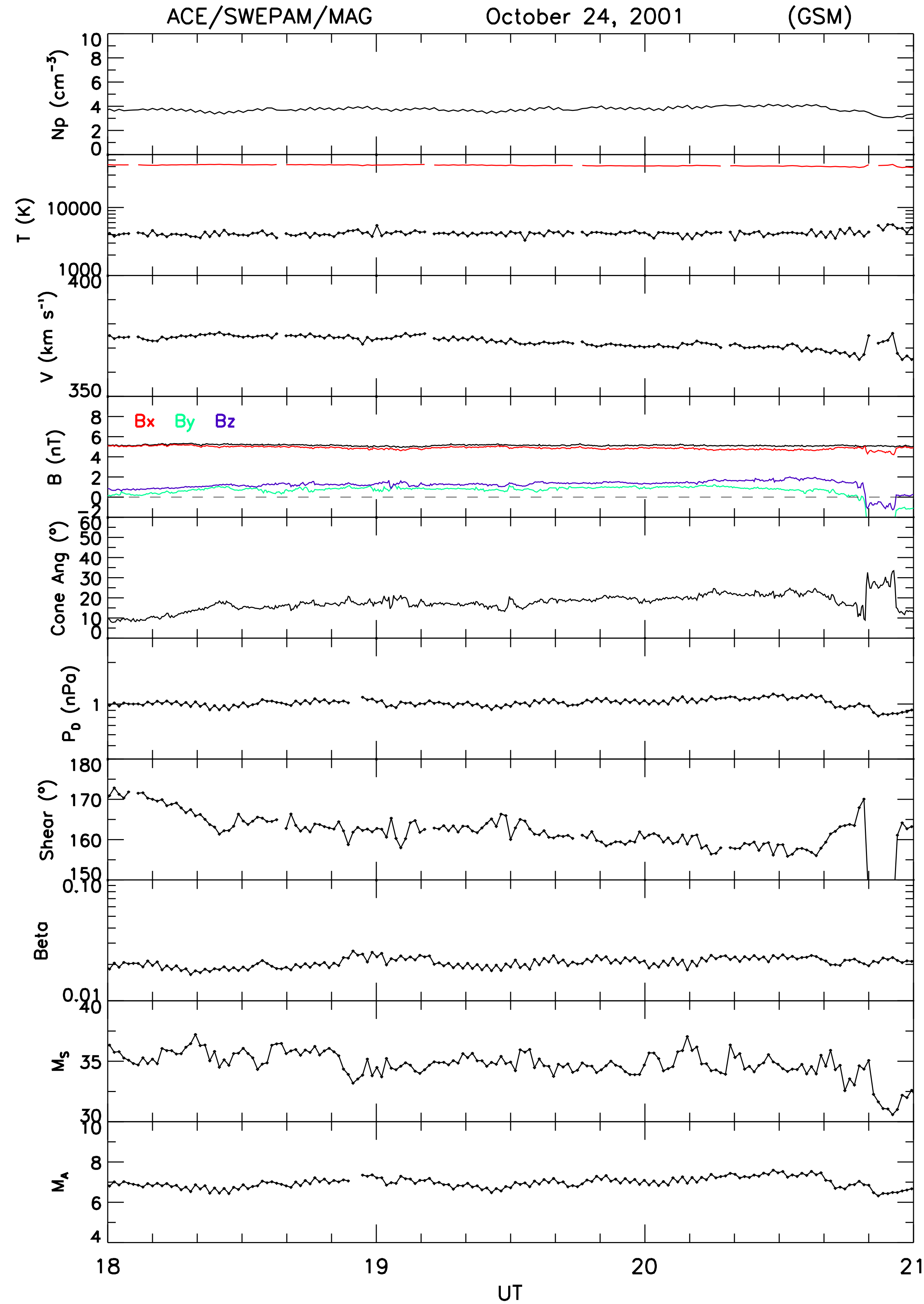
ACE/SWEPAM/MAG
October 24, 2001
(GSM)
Np (cm^{-3})
10
8
6
4
2
0
T (K)
10000
1000
V (km s^{-1})
400
350
B (nT)
Bx
By
Bz
8
6
4
2
0
-2
Cone Ang (°)
60
50
40
30
20
10
0
P_D (nPa)
1
Shear (°)
180
170
160
150
Beta
0.10
0.01
M_S
40
35
30
M_A
10
8
6
4
18
19
20
21
UT

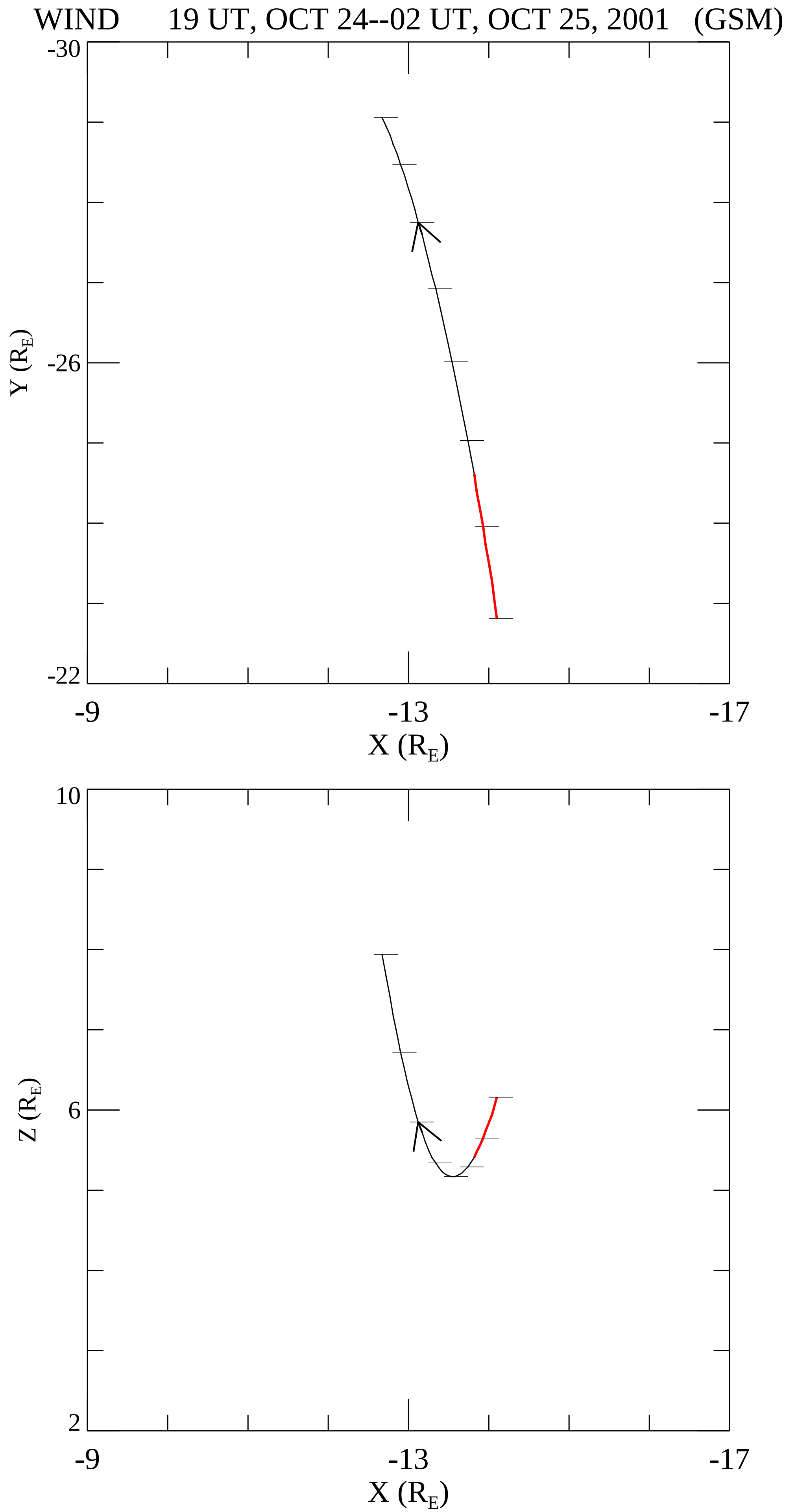

WIND 19 UT, OCT 24--02 UT, OCT 25, 2001 (GSM)
-30
-26
-22
Y (R_E)
-9
-13
-17
X (R_E)
10
6
2
Z (R_E)
-9
-13
-17
X (R_E)

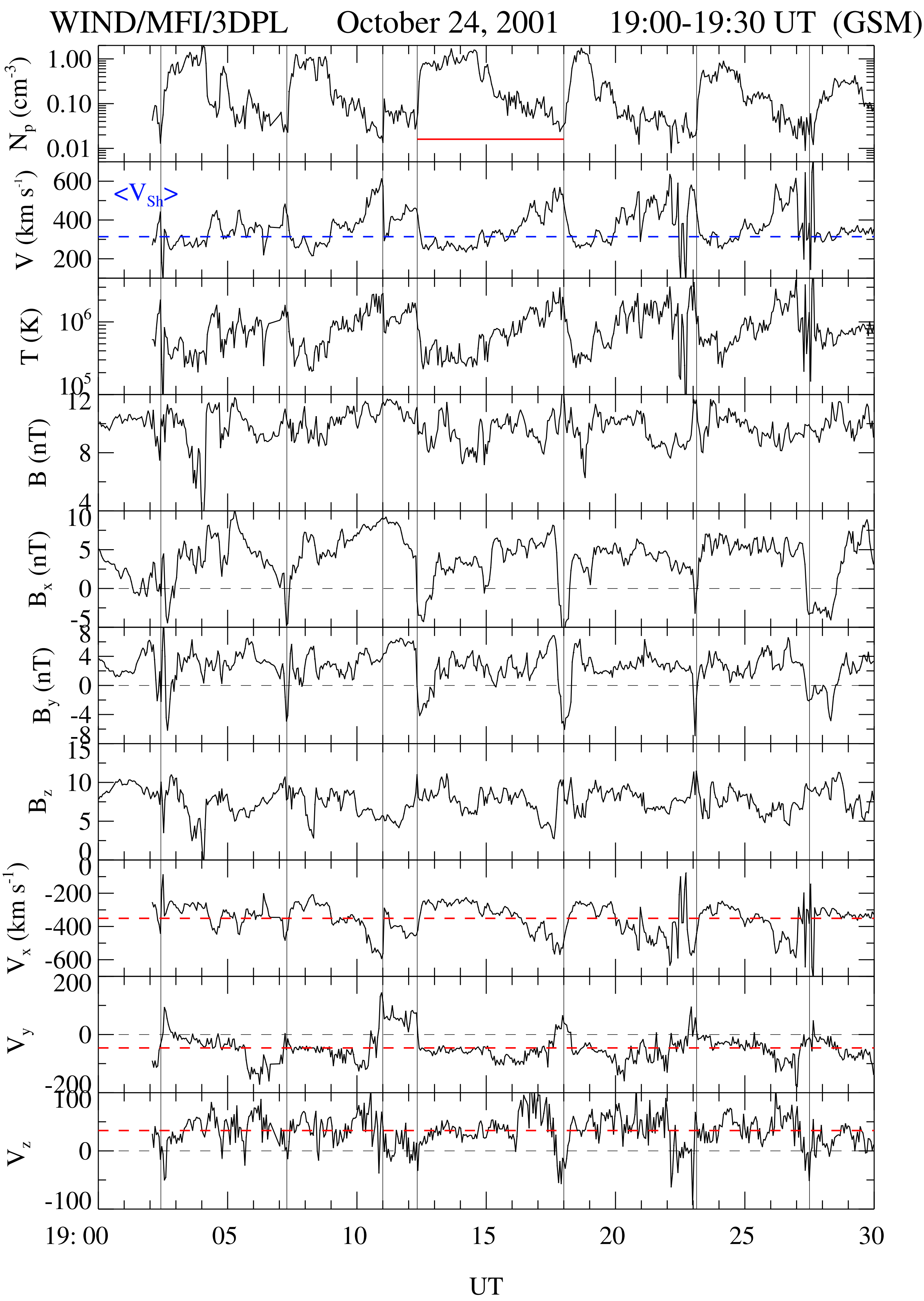
WIND/MFI/3DPL October 24, 2001 19:00-19:30 UT (GSM)
N_p (cm^{-3})
<V_{Sh}>
V (km s^{-1})
T (K)
B (nT)
B_x (nT)
B_y (nT)
B_z
V_x (km s^{-1})
V_y
V_z
19: 00
05
10
15
20
25
30
UT

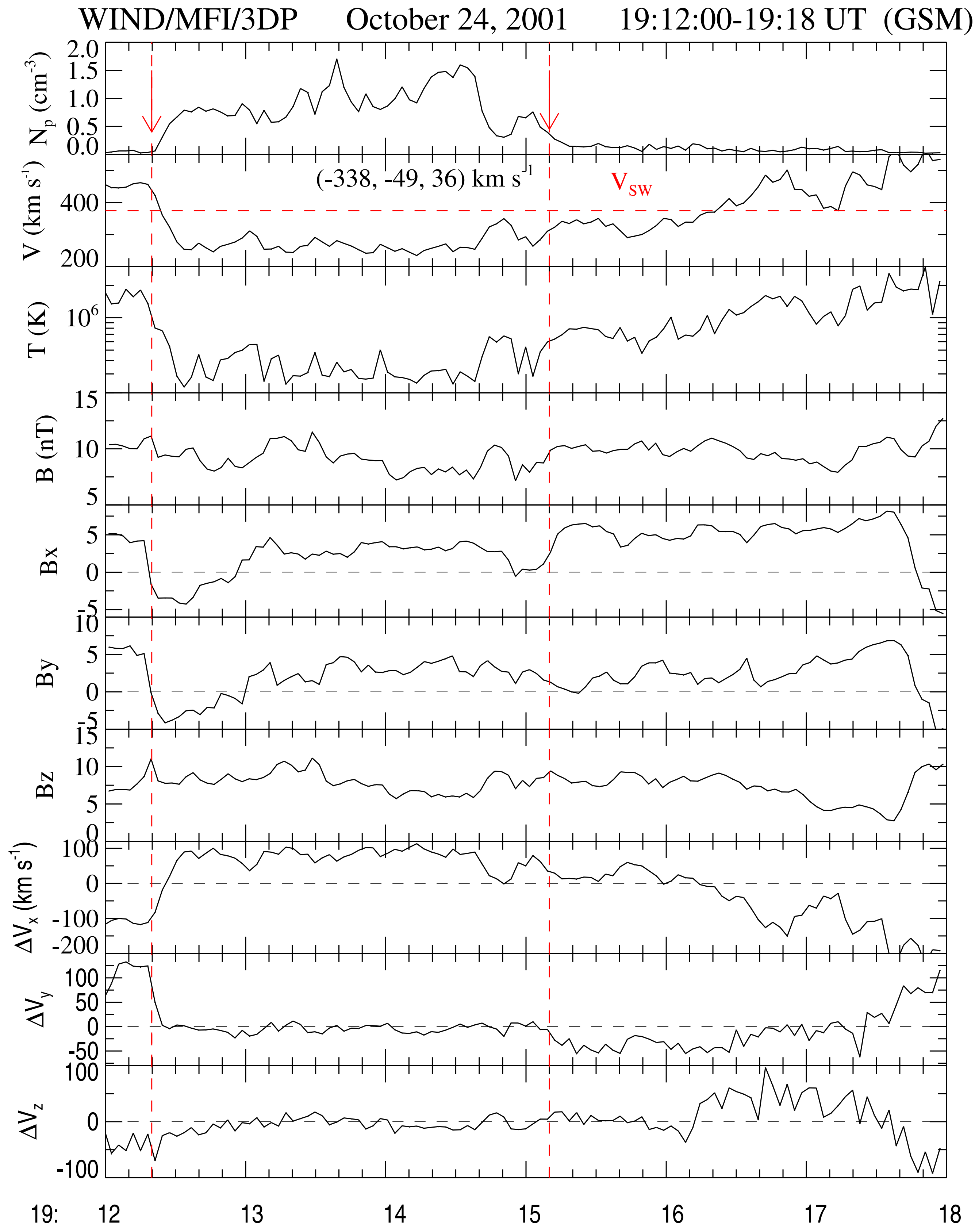
WIND/MFI/3DP October 24, 2001 19:12:00-19:18 UT (GSM)
N_p (cm^-3)
V (km s^-1)
(-338, -49, 36) km s^-1
V_SW
T (K)
B (nT)
Bx
By
Bz
ΔV_x (km s^-1)
ΔV_y
ΔV_z
19: 12 13 14 15 16 17 18
UT

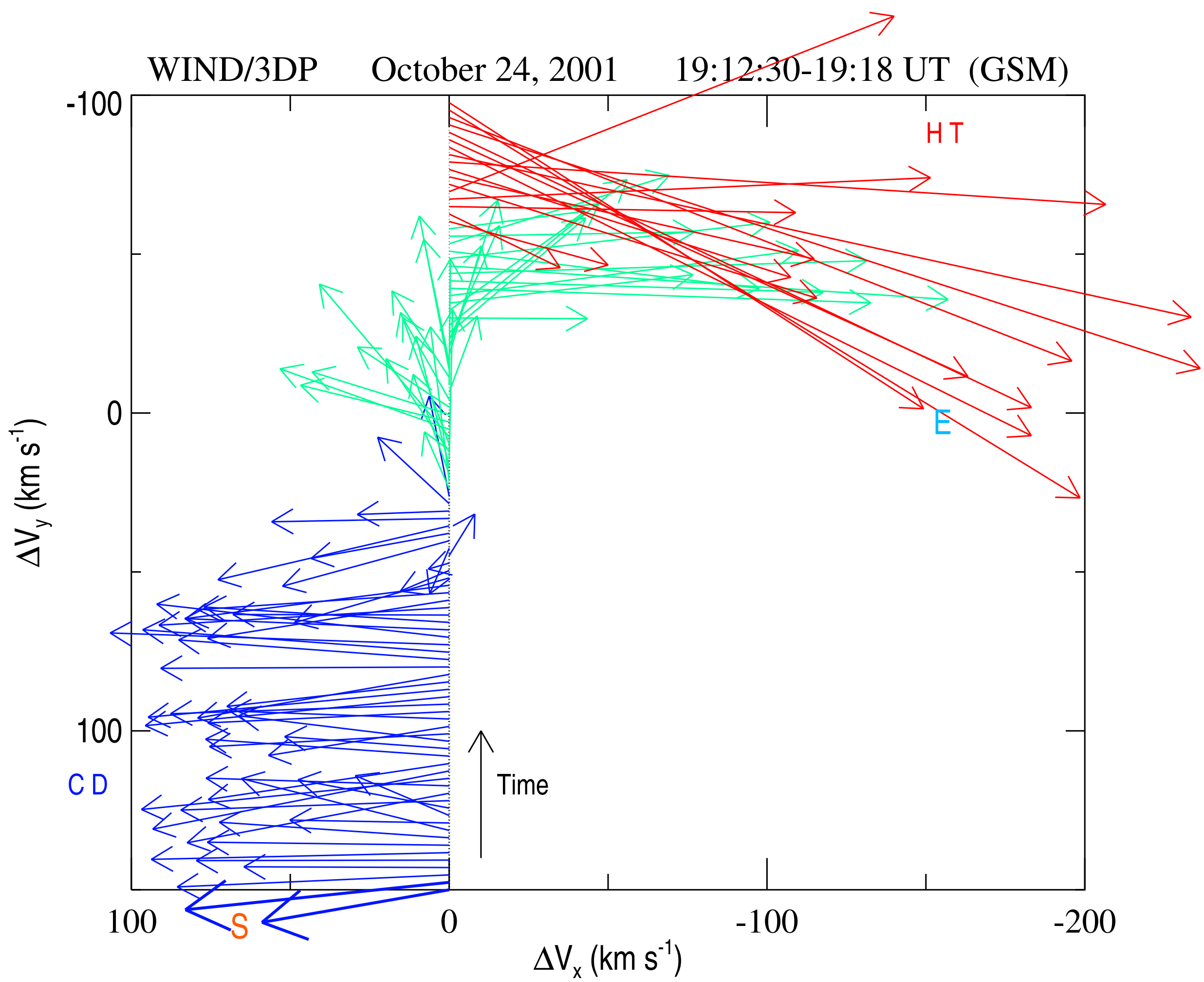

WIND/3DP October 24, 2001 19:12:30-19:18 UT (GSM)
-100
0
100
ΔV_y (km s^{-1})
100
0
-100
-200
ΔV_x (km s^{-1})
HT
E
CD
S
Time

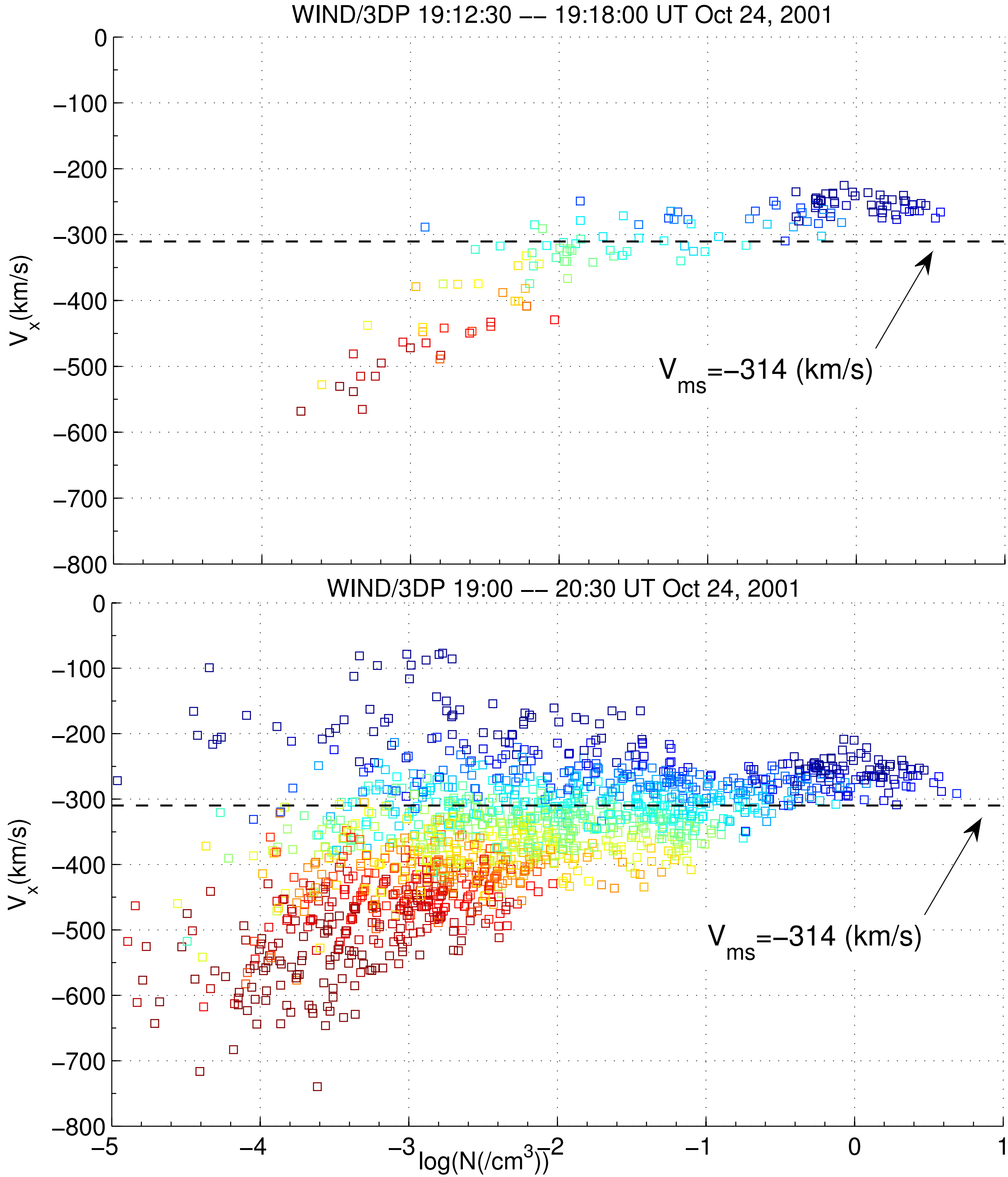

WIND/3DP 19:12:30 -- 19:18:00 UT Oct 24, 2001
V_x(km/s)
V_{ms}=−314 (km/s)
0
−100
−200
−300
−400
−500
−600
−700
−800
WIND/3DP 19:00 -- 20:30 UT Oct 24, 2001
V_x(km/s)
V_{ms}=−314 (km/s)
0
−100
−200
−300
−400
−500
−600
−700
−800
−5
−4
−3
−2
−1
0
1
log(N(/cm^3))

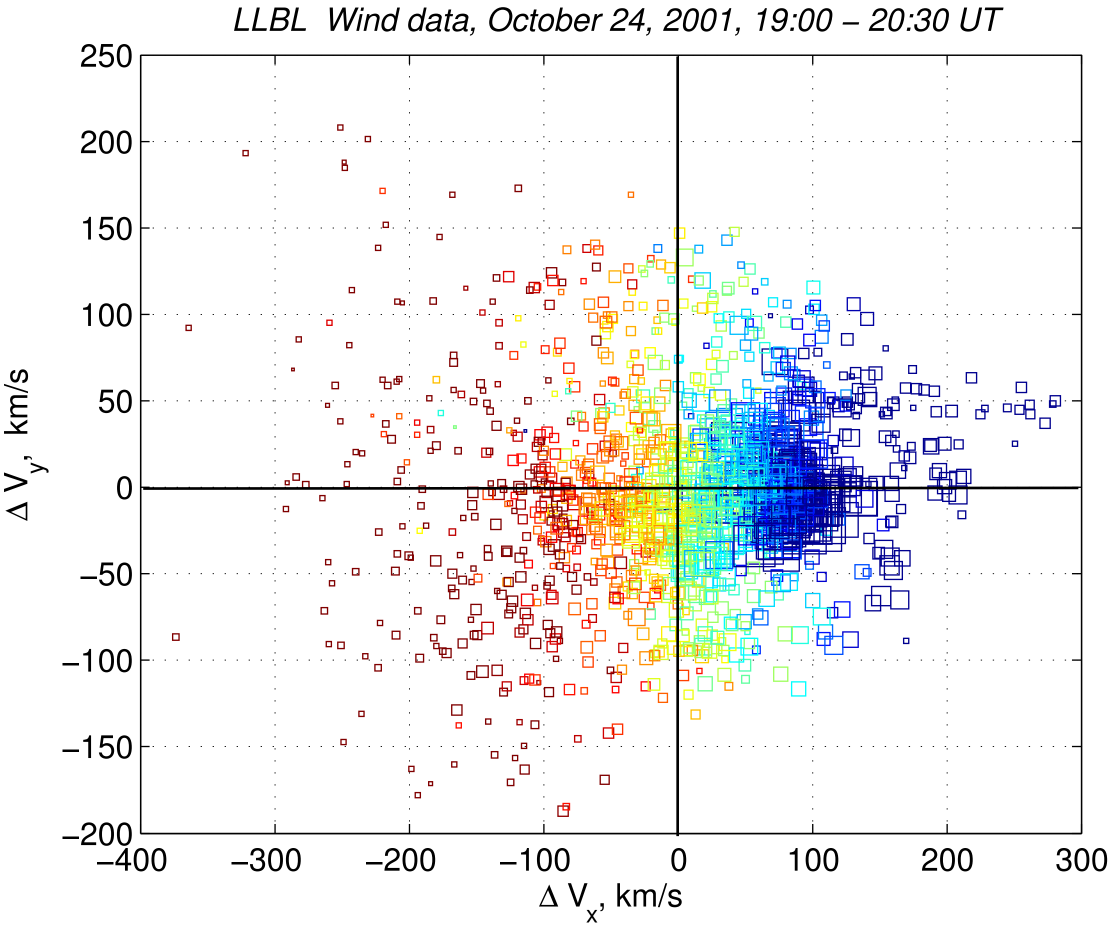

LLBL Wind data, October 24, 2001, 19:00 – 20:30 UT
250
200
150
100
50
0
−50
−100
−150
−200
Δ V_y, km/s
−400
−300
−200
−100
0
100
200
300
Δ V_x, km/s

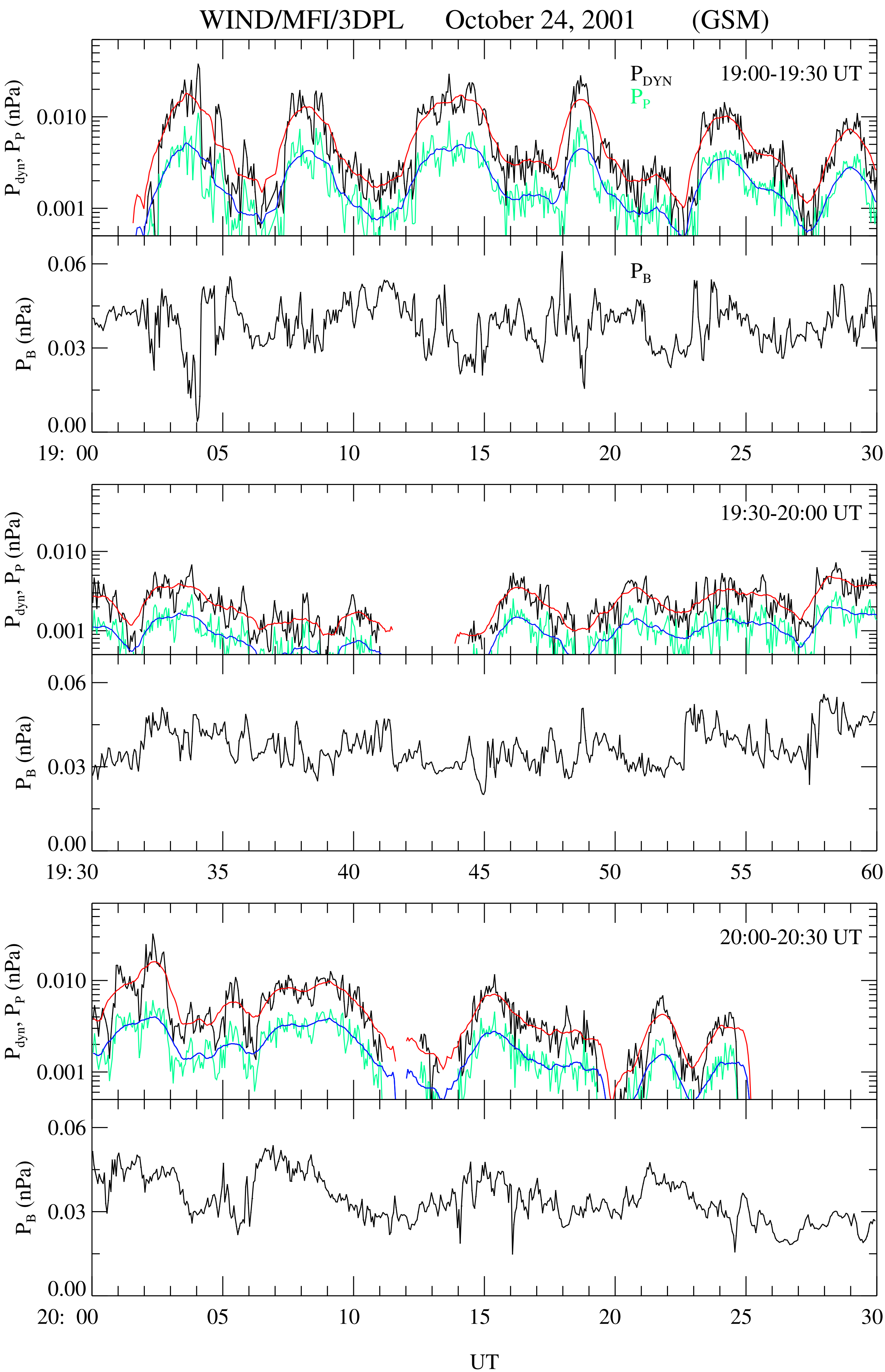

WIND/MFI/3DPL October 24, 2001 (GSM)
P_{DYN}
P_P
19:00-19:30 UT
P_{dyn}, P_P (nPa)
0.010
0.001
P_B
P_B (nPa)
0.06
0.03
0.00
19: 00
05
10
15
20
25
30
19:30-20:00 UT
19: 30
35
40
45
50
55
60
20:00-20:30 UT
20: 00
UT

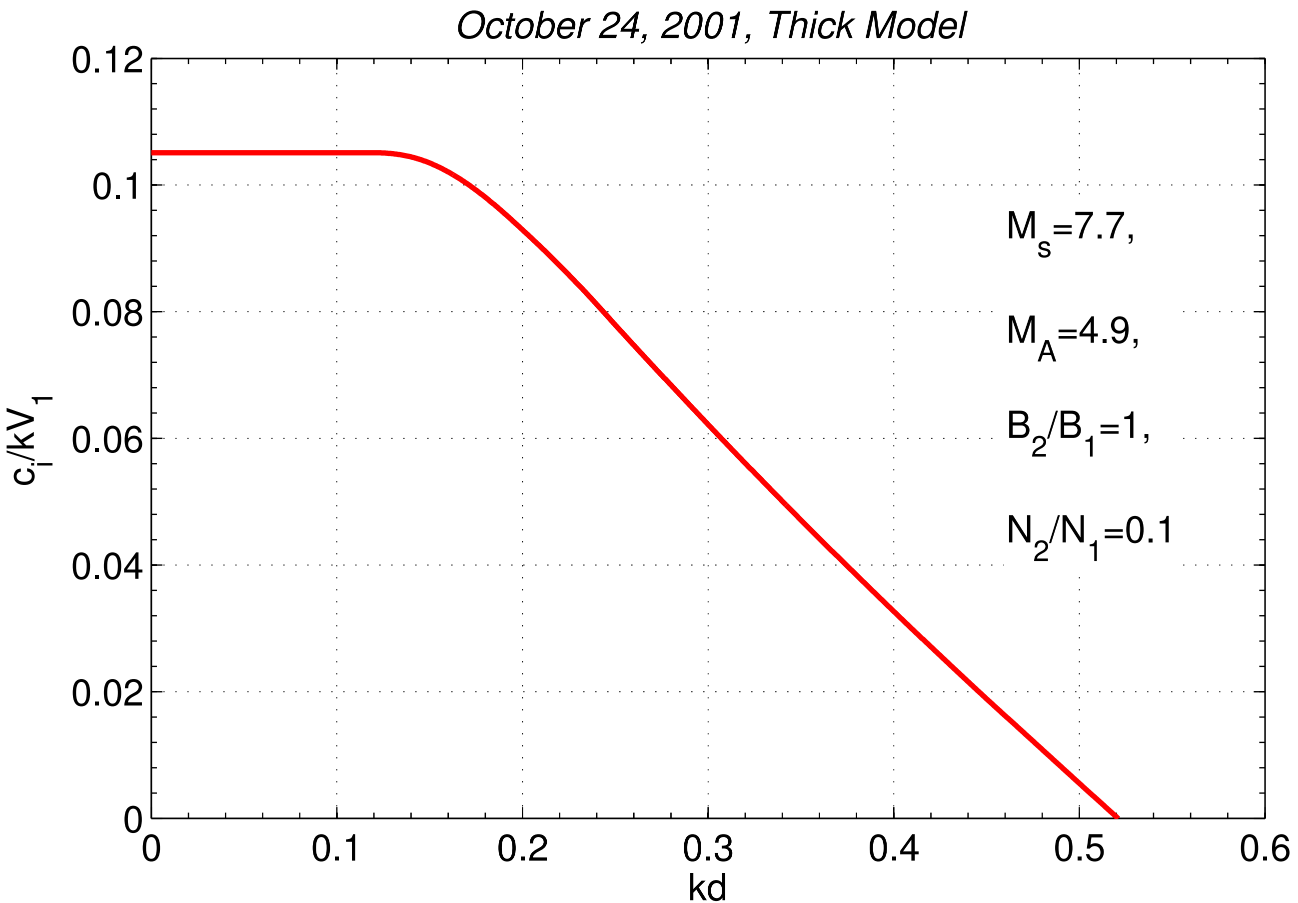

October 24, 2001, Thick Model
0.12
0.1
0.08
0.06
0.04
0.02
0
c_i/kV_1
0
0.1
0.2
0.3
0.4
0.5
0.6
kd
M_s=7.7,
M_A=4.9,
B_2/B_1=1,
N_2/N_1=0.1

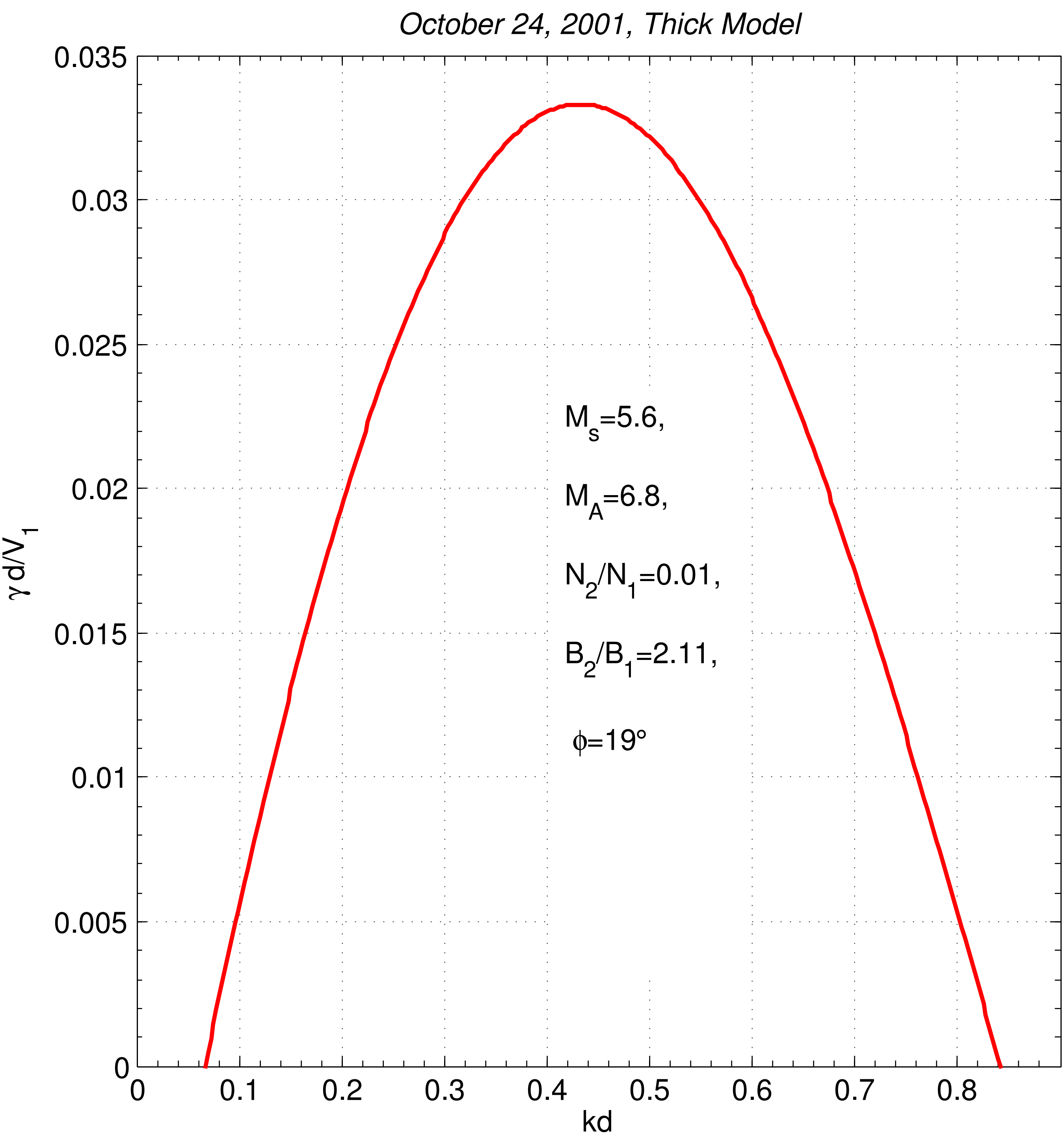

October 24, 2001, Thick Model
0.035
0.03
0.025
0.02
0.015
0.01
0.005
0
γ d/V1
0
0.1
0.2
0.3
0.4
0.5
0.6
0.7
0.8
kd
Ms=5.6,
MA=6.8,
N2/N1=0.01,
B2/B1=2.11,
φ=19°